

离子对UIO-66-2OH光催化性能的影响

李石雄^{*,1,2} 黄凤兰¹ 宾月景¹ 韦玉彩¹ 唐雪丽¹ 廖蓓玲^{*,2}

(¹梧州学院化学工程与资源再利用学院,梧州 543002)

(²河池学院化学与生物工程学院,河池 546300)

摘要: 实际废水中存在的离子会对有机污染物的光催化降解产生影响。以ZrCl₄和2,5-二羟基对苯二甲酸为原料,通过水热合成法成功制备了金属有机骨架材料UIO-66-2OH。通过红外(IR)、X射线粉末衍射(XRD)、X射线光电子能谱(XPS)和扫描电子显微镜(SEM)对UIO-66-2OH的结构进行表征。利用水中常见的金属阳离子和无机阴离子,探索UIO-66-2OH的光催化性能。研究发现,金属阳离子Fe³⁺和无机阴离子HCO₃⁻、CO₃²⁻可以加快光催化降解的速度。然而,金属离子Na⁺、K⁺、Ca²⁺、Mg²⁺、Cu²⁺和无机阴离子Cl⁻、SO₄²⁻、PO₄³⁻会抑制光催化性能,且离子价态越高,抑制效果越明显。

关键词: 光催化; UIO-66-2OH; 离子影响; 性能

中图分类号: O614.81⁺2; O614.24⁺1; O614.24⁺2

文献标识码: A

文章编号: 1001-4861(2021)08-1465-10

DOI: 10.11862/CJIC.2021.173

Effect of Ions on Photocatalytic Performance of UIO-66-2OH

LI Shi-Xiong^{*,1,2} HUANG Feng-Lan¹ BIN Yue-Jing¹ WEI Yu-Cai¹ TANG Xue-Li¹ LIAO Bei-Ling^{*,2}

(¹School of Chemical Engineering and Resource Recycling, Wuzhou University, Wuzhou, Guangxi 543002, China)

(²School of Chemistry and Biological Engineering, Hechi University, Hechi, Guangxi 546300, China)

Abstract: Photocatalytic degradation of organic pollutants in actual wastewater requires exploring the influence of ions on the performance of photocatalysts. In this work, ZrCl₄ and 2,5-dihydroxyterephthalic acid were used as raw materials, and the metal-organic framework material UIO-66-2OH was successfully prepared by the hydrothermal synthesis method. The structure of UIO-66-2OH was characterized by infrared (IR), X-ray powder diffraction (XRD), X-ray photoelectron spectroscopy (XPS), and scanning electron microscope (SEM). The photocatalytic performance of UIO-66-2OH was explored by using common metal cations and inorganic anions in water. The studies have found that metal cations Fe³⁺ and inorganic anions HCO₃⁻ and CO₃²⁻ can accelerate the rate of photocatalytic degradation. However, the metal ions Na⁺, K⁺, Ca²⁺, Mg²⁺, Cu²⁺ and inorganic anions Cl⁻, SO₄²⁻, PO₄³⁻ can inhibit the photocatalytic performance, and the higher the ion valence, the more obvious the inhibition effect.

Keywords: photocatalytic; UIO-66-2OH; ions effect; performance

0 Introduction

The photocatalytic oxidation technology has the characteristics of low energy consumption and mild re-

action conditions, it is an effective method to solve organic pollution in water^[1-5]. Since TiO₂ can decompose water to prepare H₂^[6], the photocatalytic technology has been receiving extensive attention and research.

收稿日期: 2021-03-02。收修改稿日期: 2021-06-22。

广西科技基地和人才专项(No.AD19245031)、梧州学院校级科研项目(博士基金项目)(No.2020A001)、梧州学院人才引进科研启动基金(No.WZUQDJJ21081)、梧州市科技项目(No.2020006)和梧州学院开放实验室创新性实验(No.201900005)资助。

*通信联系人。E-mail: lxs1324@163.com, liaobeiling1324@163.com

With the efforts of scientists, many inorganic and metal organic frameworks photocatalysts have been discovered and developed. They mainly include $\text{ZnO}^{[7]}$, $\text{CdS}^{[8]}$, $\text{Fe}_2\text{O}_3^{[9]}$, $\text{MoS}_2^{[10]}$, $\text{WS}_2^{[11]}$, BiOX ($\text{X}=\text{Cl}, \text{Br}, \text{I}$)^[12], UIO-66-X ($\text{X}=\text{H}, \text{OH}, \text{NH}_2, \text{NO}_2$)^[13], MIL-101(Fe)-X ($\text{X}=\text{H}, \text{NH}_2, \text{NO}_2$)^[14], $\text{MIL-125(Ti)-NH}_2^{[15]}$, $\text{MIL-53(Fe)}^{[16]}$, and $\text{MIL-88B(Fe)}^{[17]}$. Among these photocatalysts, there are many photocatalysts with good photocatalytic performance and potential for practical application. The MOFs catalyst is one of them. They have the advantages of large specific surface area, good stability, and easy control of the structure. They have shown great potential for applications in light and electrocatalysis^[18-20]. For example, it is used to catalyze the production of hydrogen, the reduction of CO_2 , and the degradation of organic pollutants^[2-4,21]. Regrettably, many studies do not consider the complexity of actual wastewater. The composition of the organic matter in the actual wastewater is complex^[22-24], the pH of the solution varies greatly, and the metal cations and inorganic anions vary widely and have different concentrations. Therefore, to pursue the application research of photocatalysts, it is necessary to study the influence of organic pollutant concentration, pH of solution and ions.

In this work, the UIO-66-2OH photocatalyst was successfully prepared by the hydrothermal synthesis method and its structure was characterized. The effects of pH, ion species and concentration of the solution on the photocatalytic performance of UIO-66-2OH were explored by using methylene blue (MB) as an organic pollutant in water.

1 Experimental

1.1 Instruments and reagents

The Nicolet 5DX FT-IR spectrometer was used to characterize and test the presence of hydroxyl functional groups in the UIO-66-2OH photocatalyst. The structure of UIO-66-2OH photocatalyst was tested and analyzed by using Rigaku's D/max 2500 X-ray powder diffractometer (XRD). The test conditions were as follows: $\text{Cu K}\alpha$ ($\lambda=0.156\ 04\ \text{nm}$), tube voltage was 40 kV, tube current was 150 mA, graphite monochromator, 2θ was 5° to 65° . The composition and valence state of the ele-

ments in UIO-66-2OH photocatalyst were determined by using the ESCALAB250 X-ray photoelectron spectroscopy (XPS) of Thermo Fisher Scientific with a base pressure of 1.33×10^{-7} Pa. The morphology of UIO-66-2OH photocatalyst was observed by the Hitachi SU8010 scanning electron microscope (SEM), the acceleration voltage during the test was 1.0 kV. The light absorption behavior of UIO-66-2OH photocatalyst was tested and analyzed by using UV-2700 from SHIMADZU of Japan, BaSO_4 as a reference. The specific surface area of UIO-66-2OH photocatalyst was calculated from N_2 adsorption-desorption data gained at 77 K by AUTO CHEM II 2920 from American Micro Instrument Company. The visible light photocatalytic reaction required in the experiment was carried out on a 1 000 W xenon lamp catalytic reactor.

The chemical reagents used in the experiment, such as MB, ZrCl_4 , terephthalic acid, 2-aminoterephthalic acid, 2, 5 - dihydroxyterephthalic acid, *N,N* - dimethylamide (DMF), methanol, chloride and sodium salts, all of them are analytically pure reagents, produced by Energy Chemical Co., Ltd (Shanghai, China). The pure water used in the experiment was prepared by reverse osmosis in the laboratory.

1.2 Synthesis of UIO-66

UIO-66 was synthesized according to the method reported in the literature^[2]. A mixture of ZrCl_4 (3.495 g, 15 mmol) and terephthalic acid (2.491 g, 15 mmol) in 115 mL DMF was dissolved by ultrasonic wave. After the mixed solution was evenly dispersed, it was sealed in a 250 mL polytetrafluoroethylene (PTFE) reactor and heated in an oven at $120\ ^\circ\text{C}$ for 24 h. After the reaction, it was cooled to room temperature, the solvent was removed by centrifugation, and the white solid powder obtained was collected. The white solid powder was collected and washed three times with DMF and methanol, and dried in a vacuum drying oven at $120\ ^\circ\text{C}$ for 16 h. Finally, the UIO-66 white powder was obtained.

1.3 Synthesis of UIO-66-NH_2

UIO-66-NH_2 was also synthesized according to the method reported in the literature^[2]. The procedures were similar to those in the synthesis of UIO-66 except that the organic ligand was 2-amino terephthalic acid.

1.4 Synthesis of UIO-66-2OH

UIO-66-2OH was synthesized by performing ligand exchange during hydrothermal synthesis. The specific steps were as follows: a mixture of UIO-66 (1.000 g) and 2,5-dihydroxyterephthalic acid (1.980 g, 10 mmol) in 80 mL DMF was sealed in a 250 mL PTFE reactor and heated in an oven at 120 °C for 72 h. After the reaction, it was cooled to room temperature, and the organic solvent was removed by centrifugation and the yellow powder was collected. The yellow powder was collected and washed three times with DMF and methanol, and dried in a vacuum drying oven at 120 °C for 16 h. Finally, UIO-66-2OH was obtained.

1.5 Photocatalysis experiment

The photocatalytic properties of UIO-66-2OH were studied by using UIO-66-NH₂ as reference photocatalysts, and the MB as organic pollutants. The specific process of the photocatalysis experiment was as follows: the dosage of photocatalyst was 0.010 0 g; the initial concentration of MB was $c_0=10 \text{ mg}\cdot\text{L}^{-1}$, and the dosage was 50 mL; the pH value during the photocatalysis experiment was 3, 5, 7, 9 and was measured with a Mettler pH meter; the photocatalytic reaction was carried out using an 800 W xenon lamp (A UV filter was added to the source to ensure removal the light of below 420 nm before the start of the photocatalytic reaction. At this time, the light irradiation intensity measured by the photometer was about $15 \text{ W}\cdot\text{m}^{-2}$). After the photocatalytic reaction was carried out for a certain period of time, the absorbance of MB in the solution was measured at 664 nm using an ultraviolet-visible spectrophotometer. The corresponding concentration of MB was calculated by the standard curve $A=0.070 8c+0.000 8$ ($R^2=0.999 8$), where A is the absorbance and c is the concentration. The photocatalytic degradation performance was evaluated by the change of MB concentration before and after the reaction. The degradation rate was calculated as follows:

$$R=(1-\frac{c_t}{c_0})\times 100\%$$

Where R is the degradation rate (%), c_0 is the initial concentration of MB and c_t is the concentration of MB at t for adsorption and degradation experiment ($\text{mg}\cdot\text{L}^{-1}$).

2 Results and discussion

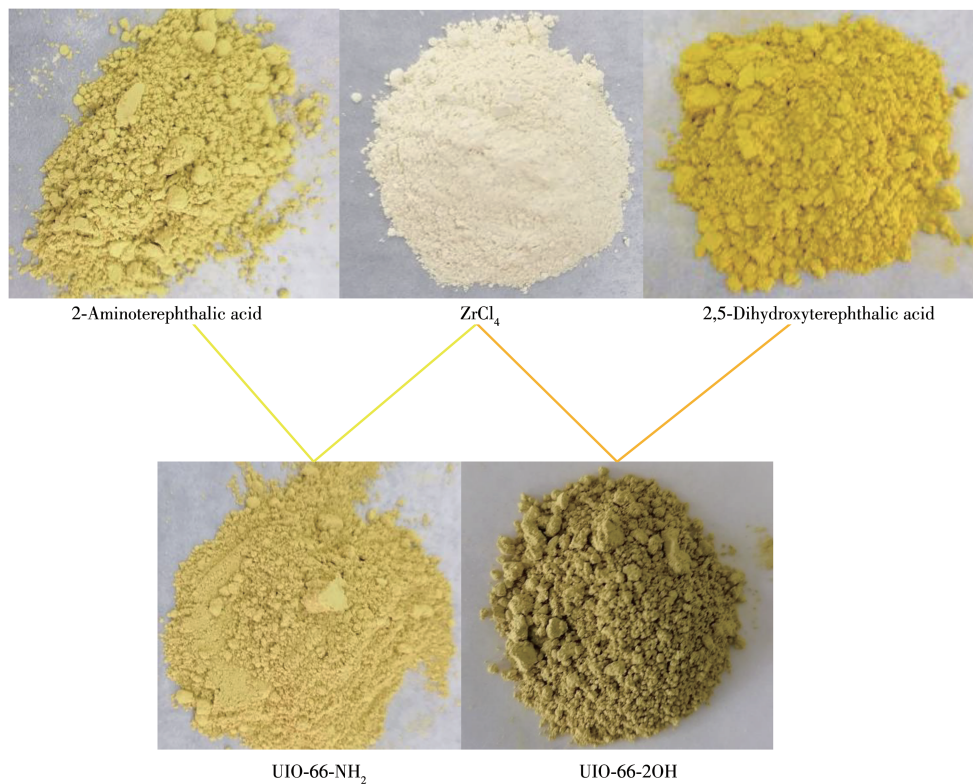
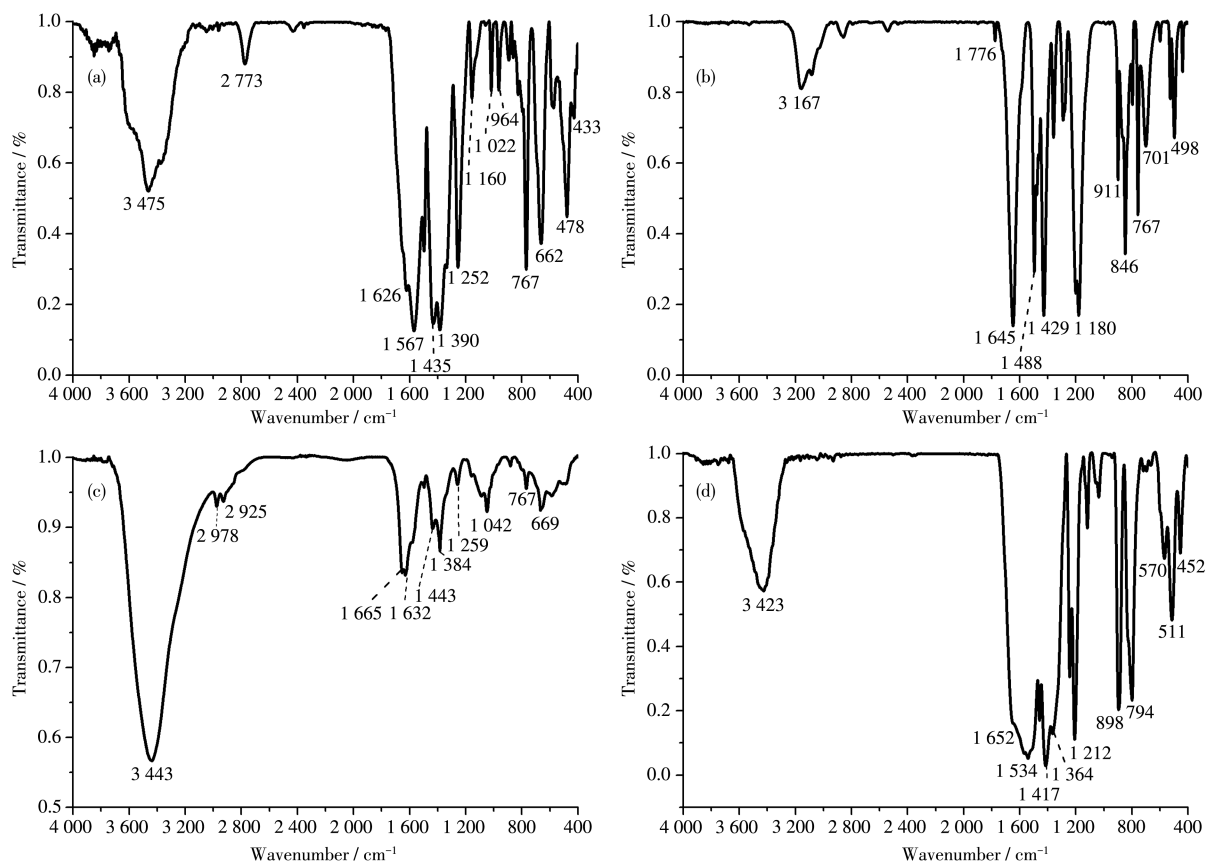
2.1 Structure of UIO-66-2OH

UIO-66-NH₂ and UIO-66-2OH were successfully synthesized by hydrothermal synthesis. It can be clearly seen from Fig.1 that the light yellow powder of 2-aminoterephthalic acid (Fig. 1a) reacted with the white powder of ZrCl₄ (Fig. 1b) to form yellow powder UIO-66-NH₂ (Fig. 1d). However, the yellow powder of 2,5-dihydroxyterephthalic acid (Fig. 1c) reacted with the white powder of ZrCl₄ (Fig. 1b) to form tan powder UIO-66-2OH (Fig. 1e). It can be seen that modifying the organic ligand can regulate the color change of metal organic frameworks (MOFs). The structure of UIO-66-2OH was characterized by FT-IR, XRD, SEM, and XPS.

2.1.1 IR

The IR characterization analysis of the photocatalyst can determine the functional groups contained in its structure. Fig.2 is the IR spectra of 2-aminoterephthalic acid, 2,5-dihydroxyterephthalic acid, UIO-66-NH₂, and UIO-66-2OH. In general, the $\nu(\text{C}=\text{O})$ characteristic absorption peak in the organic carboxylic acid is at $1\ 691 \text{ cm}^{-1}$. However, the IR spectrum (Fig. 2c) of UIO-66-NH₂ showed that the $\nu(\text{C}=\text{O})$ peak have shifted to low frequency of $1\ 665 \text{ cm}^{-1}$. The characteristic absorption peak at $3\ 443 \text{ cm}^{-1}$ can be attributed as the $\nu(\text{N}-\text{H})$ stretching peak. The characteristic absorption peak at $1\ 632 \text{ cm}^{-1}$ can be attributed as the $\nu(\text{N}-\text{H})$ in-plane bending vibration peak. The characteristic absorption peak at $1\ 259 \text{ cm}^{-1}$ can be attributed as the $\nu(\text{C}-\text{N})$ stretching vibration peak. The characteristic absorption peak at 669 cm^{-1} can be attributed as the out-of-plane bending vibration peak of $\nu(\text{N}-\text{H})$.

The IR characterization analysis (Fig. 2d) of UIO-66-2OH showed that —OH was also successfully introduced. The IR absorption peak at $3\ 423$ and $1\ 364 \text{ cm}^{-1}$ can be attributed to the characteristic absorption peak of $\nu(\text{—OH})$. The absorption peaks at $1\ 652$ and $1\ 212 \text{ cm}^{-1}$ can be attributed to the characteristic absorption peak of $\nu(\text{C}=\text{O})$. These functional groups are similar to those reported in the literature^[25]. The above IR data indicate that 2,5-dihydroxyterephthalic acid has reacted with Zr(IV) to form complex.

Fig.1 Colors of reagents, UIO-66-NH₂ and UIO-66-2OHFig.2 IR spectra of (a) 2-aminoterephthalic acid, (b) 2,5-dihydroxyterephthalic acid, (c) UIO-66-NH₂, and (d) UIO-66-2OH

2.1.2 XRD

The XRD can be used to characterize and analyze the crystal structure of the photocatalyst (Fig. 3). The peaks at 7.6° , 8.7° , 12.3° , 14.3° , 14.9° , 17.2° , 18.6° , 19.3° , 21.2° , 22.4° , 24.1° , 25.9° , 28.3° , 29.9° , 30.9° , 32.3° , 33.3° , 35.8° , 37.6° , 39.5° , 40.8° , 43.4° , and 44.5° are corresponding to the simulated UIO-66^[2]. The results shows that UIO-66-NH₂ and UIO-66-2OH have been successfully synthesized.

2.1.3 XPS

The XPS can be used to analyze the element composition and valence states of the photocatalyst. The XPS spectrum of UIO-66-2OH shows that it is composed of Zr, C, and O (Fig. 4a). The characteristic peak at 283.56, 830.46, 182.90, and 185.42 eV are attributed

to C1s, O1s, Zr3d_{5/2}, and Zr3d_{3/2} orbitals of UIO-66-2OH, respectively (Fig. 4b~4d). Therefore, the metal ion in UIO-66-2OH is Zr(IV).

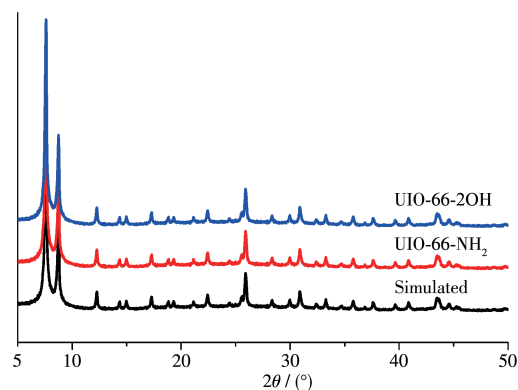


Fig.3 XRD patterns of UIO-66-2OH and UIO-66-2OH and simulated pattern

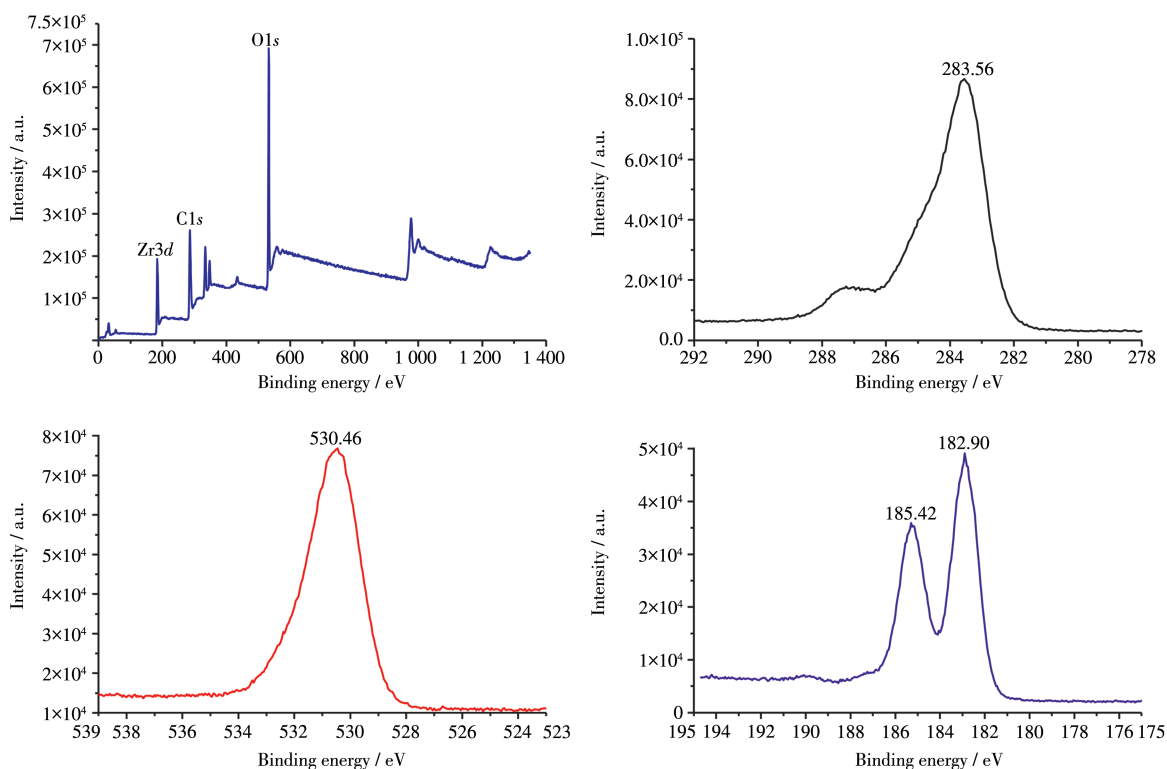


Fig.4 XPS spectra of UIO-66-2OH: (a) survey spectrum; (b) C1s; (c) O1s; (d) Zr3d

2.1.4 SEM

The particle size of the photocatalyst can affect the catalytic performance. The SEM images of UIO-66-2OH showed that the particle with a size of about 200 nm was uniform and the shape was roughly oval (Fig.5).

2.2 N₂ adsorption-desorption test

The specific surface area of the photocatalyst will

also affect its photocatalytic performance. The N₂ adsorption-desorption isotherm can be used to measure the specific surface area, pore size and pore volume of the photocatalyst. The test results showed that UIO-66-NH₂ and UIO-66-2OH are typical S-type adsorption curves (Fig.6 and Table 1)^[2]. It can be seen that the specific surface area of UIO-66-NH₂ ($763 \text{ m}^2 \cdot$

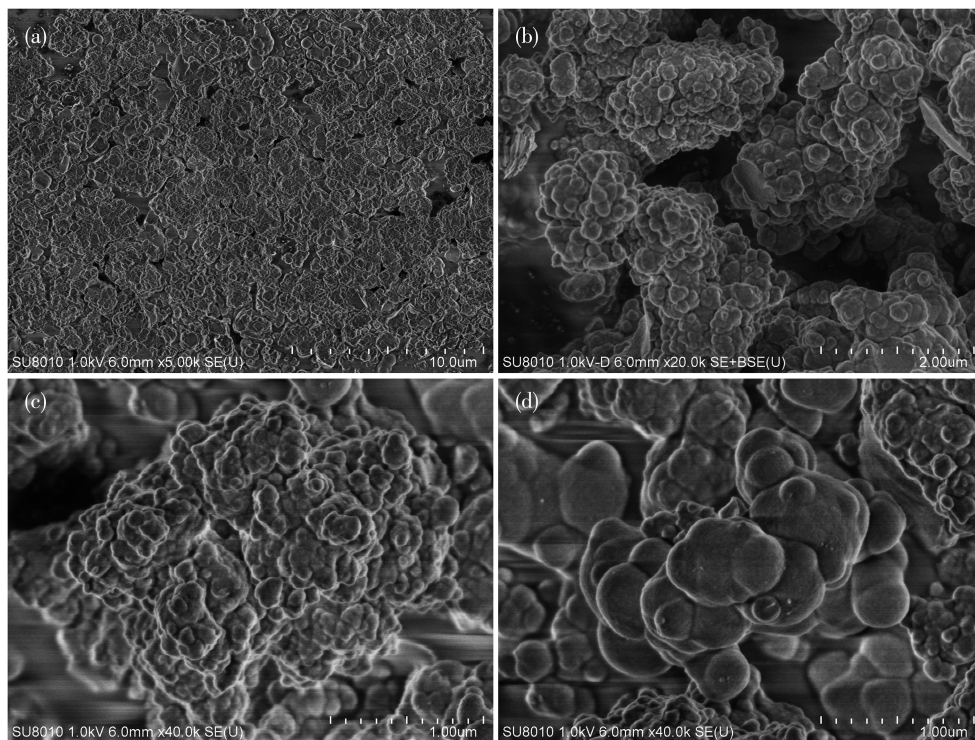
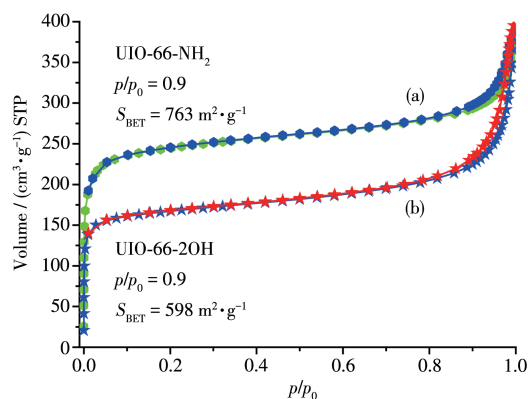


Fig.5 SEM images of UIO-66-2OH

g^{-1}) was larger than UIO-66-2OH. Though UIO-66-2OH has two $-\text{OH}$ functional groups, its specific surface area can still reach $598 \text{ m}^2 \cdot \text{g}^{-1}$.

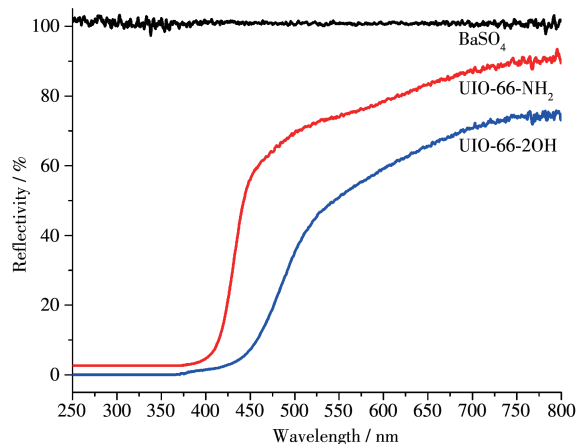
Fig.6 N_2 adsorption-desorption isotherms for UIO-66- NH_2 and UIO-66-2OHTable 1 Specific surface area, pore size, and pore volume of UIO-66- NH_2 and UIO-66-2OH

Sample	Specific surface area / ($\text{m}^2 \cdot \text{g}^{-1}$)	Pore size / nm	Pore volume / ($\text{cm}^3 \cdot \text{g}^{-1}$)
UIO-66- NH_2	763	1.567	0.340 3
UIO-66-2OH	598	1.435	0.298 7

2.3 UV-Vis DRS

The absorption of light by the photocatalyst can di-

rectly affect its performance. The UV-Vis DRS characterization of the photocatalyst can be used to judge its light absorption behavior and the choice of light source in the photocatalysis process. UIO-66- NH_2 and UIO-66-2OH had strong light absorption in both the UV and visible regions when the BaSO_4 was used as a blank control experiment (Fig. 7). UIO-66-2OH absorbed more than 50% of light in the visible light range of 400~540 nm. But, UIO-66- NH_2 absorbed light less than 50% in the visible light range of 400~445 nm.

Fig.7 UV-Vis DRS spectra of UIO-66- NH_2 and UIO-66-2OH

So, UIO-66-2OH has stronger visible light absorption than UIO-66-NH₂. Through the formula $E_g=1240/\lambda_g$, the band gap (E_g) of UIO-66-NH₂ and UIO-66-2OH can be calculated as 2.8 and 2.6, respectively. They have strong visible light absorption indicated that UIO-66-2OH can perform photocatalytic degradation experiments under visible light conditions.

2.4 Photocatalytic performance

UIO-66-NH₂ photocatalyst with visible light response has been extensively studied in photocatalytic degradation of organic pollutants. It can be used as a reference catalyst when researching new photocatalysts^[2-3,26]. Both UIO-66-2OH and UIO-66-NH₂ are MOFs constructed by derivatives of terephthalic acid and Zr(IV). In this work, UIO-66-NH₂ was used as reference photocatalysts, and MB was used as organic pollutants. The photocatalytic performance of UIO-66-2OH was studied under the condition of pH=3~9 and the coexistence of ions.

2.4.1 Effect of pH on photocatalytic performance

The specific surface areas data of UIO-66-NH₂ and UIO-66-2OH indicated that they also have a good adsorption effect on MB and can also be used to remove organic pollutants in water by adsorption. When studying the photocatalytic properties, the adsorption behavior must be discussed. Therefore, the photocatalytic properties were further evaluated by using adsorption control experiments (Fig.8). The adsorption experiments of UIO-66-NH₂ and UIO-66-2OH showed that their adsorption reached equilibrium after 120 min. The experimental results (Fig. 8a) of UIO-66-2OH adsorption of MB showed that its adsorption capacity under pH=9 was greater than that under pH=3. At pH=3, 5, 7, and 9, its adsorption rate of MB can reach 0.026 7, 0.030 7, 0.035 5, and 0.038 5 mg·L⁻¹·min⁻¹, respectively. However, under these conditions, UIO-66-NH₂ adsorption rate (Fig.8c) of MB was only 0.013 8, 0.017 2, 0.019 4, and 0.021 7 mg·L⁻¹·min⁻¹. The specific surface area of UIO-66-2OH is smaller than that of UIO-66-NH₂, but its ability to adsorb MB is stronger

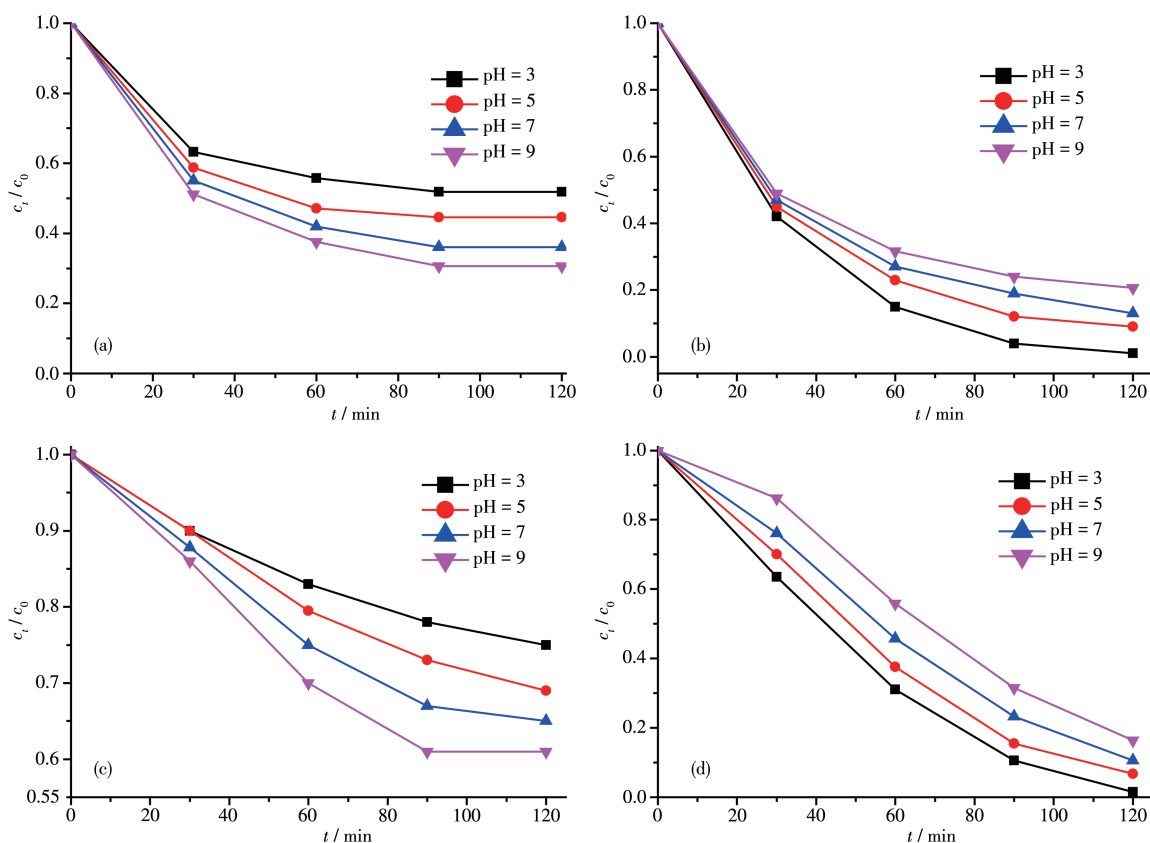


Fig.8 Adsorption performance of MB for (a) UIO-66-2OH and (c) UIO-66-NH₂; Photocatalytic degradation of MB for (b) UIO-66-2OH and (d) UIO-66-NH₂

than UIO-66-NH₂. This may be due to its structure containing two —OH functional groups. The introduction of —OH makes the surface of UIO-66-2OH more charged, which is conducive to its adsorption of MB.

The results of photocatalytic degradation of MB by UIO-66-NH₂ and UIO-66-2OH indicated that they all had good performance (Fig.8b, 8d). It can be seen from the results that the photocatalytic reaction was more favorable under acidic conditions (Fig.8b, 8d). Among them, at pH=3, the photocatalytic degradation rate was the fastest. UIO-66-2OH could degrade 50 mL of 50 mg·L⁻¹ MB solution in 90 min, while UIO-66-NH₂ needed 120 min. So, the photocatalytic degradation rates of UIO-66-2OH and UIO-66-NH₂ for MB were 0.056 and 0.042 mg·L⁻¹·min⁻¹, respectively.

2.4.2 Effect of ions on photocatalytic performance

The above photocatalytic experiment results showed that UIO-66-2OH had good photocatalytic degradation performance of organic pollutants. However, when it is put into practical application, the complexity

of actual waste water needs to be considered. For example, metal cations and inorganic anions coexist with organic pollutants in wastewater. The cation coexistence experiment at pH=7 of UIO-66-2OH showed that these metal ions showed significant impacts on the photodegradation of MB (Fig. 9). The metal ions, Na⁺ (Fig.9a), K⁺ (Fig.9b), Mg²⁺ (Fig.9c), Ca²⁺ (Fig.9d), and Cu²⁺ (Fig.9e), displayed inhibition effect in a range of 0.001~0.1 mol·L⁻¹, and the inhibition effect increased with the increase of their concentrations. This may be due to the chlorine salt used, and the Cl⁻ had a scavenging effect on the hydroxyl radicals generated in the photocatalytic process. The Fe³⁺ (Fig.9f) enhanced the degradation of MB with the increase of concentrations. This may be that there are two distinct reaction mechanisms exist in the reaction system with UIO-66-2OH and Fe³⁺: MB degradation by photogenerated holes produced by UIO-66-2OH and by ·OH produced by Fe(OH)₂⁺. As the concentration of Fe³⁺ increased in a range of 0.001~0.1 mol·L⁻¹, the Fe(OH)₂⁺ might absorb

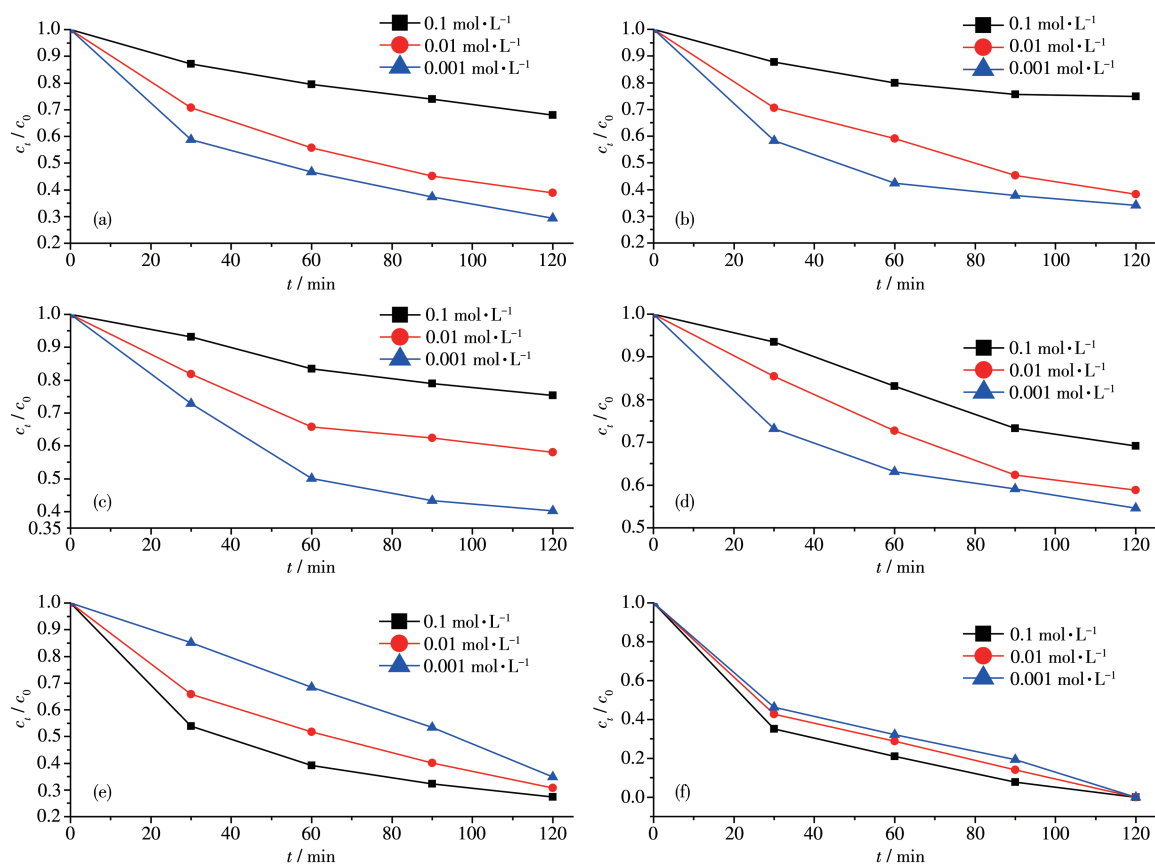


Fig.9 Effect of ions on photocatalytic performance: (a) Na⁺; (b) K⁺; (c) Mg²⁺; (d) Ca²⁺; (e) Cu²⁺; (f) Fe³⁺

most of the UV light in the solar light irradiation and be activated. With the increase of the concentration of Fe^{3+} , the photodegradation rate increased gradually due to the increase of $\cdot\text{OH}$ produced by $\text{Fe}(\text{OH})_2^{+}$ [22].

The anions of Cl^- , HCO_3^- , CO_3^{2-} , SO_4^{2-} and PO_4^{3-} are also very common in actual waste water. These inorganic anions in actual waste water also would affect the degradation rate of organic pollutants and even their degradation mechanisms. The anions coexistence experiment at pH 7 of UIO-66-2OH showed that these anions also could significantly impact on the photodegradation of MB (Fig. 10). The Cl^- displaying inhibition effect for the catalytic degradation of MB has been discussed in the above results. However, it is also a nega-

tive one-valent anion, HCO_3^- (Fig. 10a) can enhance the photocatalytic degradation of MB by UIO-66-2OH, which is similar to those reported in the literature[22]. The CO_3^{2-} (Fig. 10b) can also enhance the photocatalytic performance. But the enhancement effect was not as obvious as HCO_3^- . This may be due to the hydrolysis reaction of CO_3^{2-} and the formation of HCO_3^- . The SO_4^{2-} (Fig. 10c) and PO_4^{3-} (Fig. 10d) inhibited the photodegradation of MB, and the inhibition effect increased with the increase of their concentrations. It is clear that PO_4^{3-} displays much stronger inhibition effect than SO_4^{2-} and Cl^- . Therefore, in PO_4^{3-} , SO_4^{2-} and Cl^- , the higher the valence of the anion, the more obvious the inhibition phenomenon.

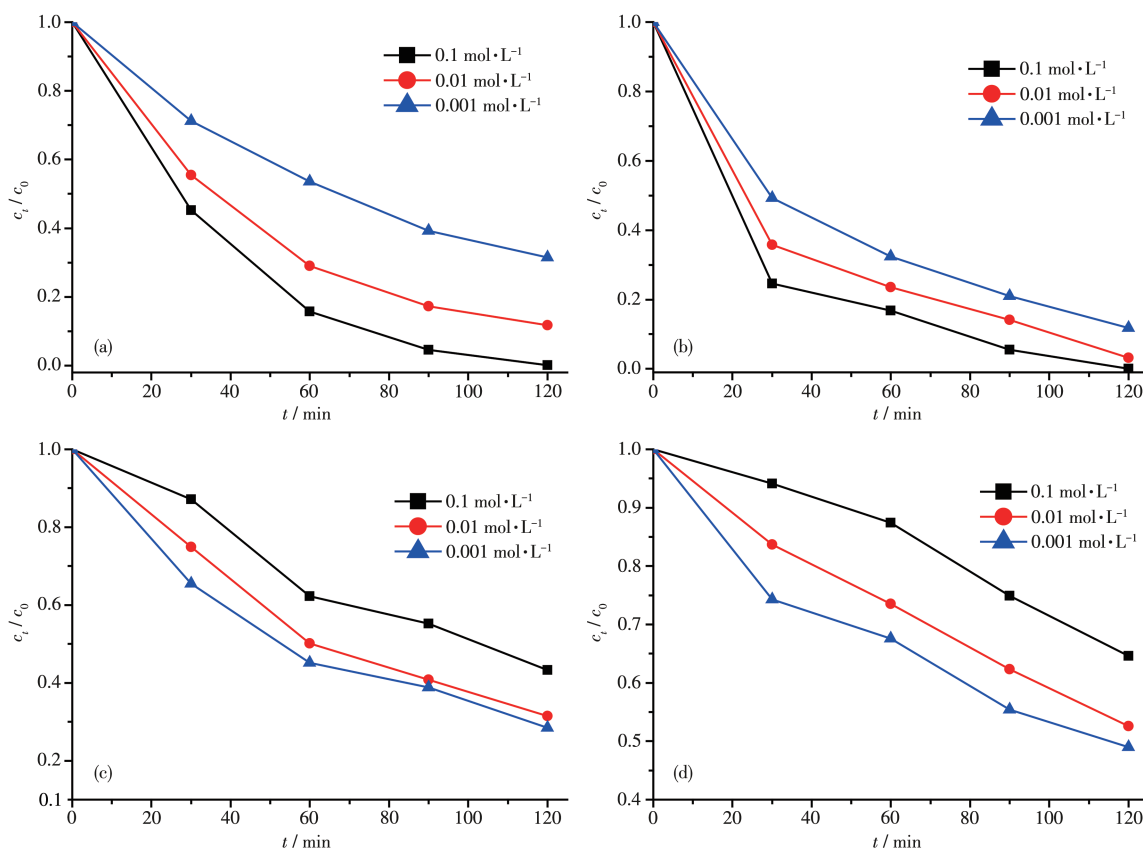


Fig. 10 Effect of anions on photocatalytic performance: (a) HCO_3^- ; (b) CO_3^{2-} ; (c) SO_4^{2-} ; (d) PO_4^{3-}

3 Conclusions

In summary, the yellow-brown powder solid photocatalyst of UIO-66-2OH was synthesized by performing ligand exchange during hydrothermal synthesis. The experiment of photocatalytic degradation of MB showed

that it had the best photocatalytic performance at pH= 3, which can reach $0.056 \text{ mg}\cdot\text{L}^{-1}\cdot\text{min}^{-1}$. However, the performance reference photocatalyst UIO-66- NH_2 was only $0.042 \text{ mg}\cdot\text{L}^{-1}\cdot\text{min}^{-1}$. The ion coexistence experiments show that the Fe^{3+} , HCO_3^- , and CO_3^{2-} can enhance the photocatalytic performance, the higher the

concentration, the more obvious the enhancement effect. While the ions of Na^+ , K^+ , Ca^{2+} , Cu^{2+} , and anions of Cl^- , SO_4^{2-} , PO_4^{3-} can inhibit the photocatalytic performance, the higher the valence, the more obvious the inhibition effect. This study clarified the results of the effects of some ions on the photocatalytic performance of UIO-66-2OH.

References:

- [1] Mamaghani A H, Haghghat F, Lee C S. *Appl. Catal. B*, **2017**,**203**:247-269
- [2] Li S X, Sun S L, Wu H Z, Wei C H, Hu Y. *Catal. Sci. Technol.*, **2018**, **8**:1696-1703
- [3] Li S X, Wei C H, Hu Y, Wu H Z, Li F S. *Inorg. Chem. Front.*, **2018**,**5**: 1282-1287
- [4] Li S X, Luo P, Wu H Z, Wei C H, Hu Y. *ChemCatChem*, **2019**,**11**: 2978-2993
- [5] Adhikar S, Kim D H. *Appl. Surf. Sci.*, **2020**,**511**:145595
- [6] Fujishima A, Honda K. *Nature*, **1972**,**238**:37-38
- [7] Elmolla E S, Chaudhuri M. *J. Hazard. Mater.*, **2010**,**173**:445-449
- [8] Cheng L, Xiang Q J, Liao Y L, Zhang H W. *Energy Environ. Sci.*, **2018**,**11**:1362-1391
- [9] Yan S D, Shi Y, Tao Y F, Zhang H. *Chem. Eng. J.*, **2019**,**359**:933-943
- [10] Lv H, Liu Y M, Tang H B, Zhang P, Wang J J. *Appl. Surf. Sci.*, **2017**, **425**:100-106
- [11] Yu W W, Chen X A, Mei W, Chen C S, Tsang Y H. *Appl. Surf. Sci.*, **2017**,**400**:129-138
- [12] Ye L Q, Su Y R, Jin X L, Xie H Q, Zhang C. *Environ. Sci. Nano*, **2014**,**1**:90-112
- [13] Shen L J, Liang R W, Luo M B, Jing F F, Wu L. *Phys. Chem. Chem. Phys.*, **2015**,**17**:117-121
- [14] Hu H, Zhang H X, Chen Y, Chen Y J, Zhuang L, Ou H. *Chem. Eng. J.*, **2019**,**368**:273-284
- [15] Wu Z Y, Huang X B, Zheng H Y, Wang P, Hai G T, Dong W J, Wang G. *Appl. Catal. B*, **2018**,**224**:479-487
- [16] Tian H L, Araya T, Li R P, Fang Y F, Huang Y P. *Appl. Catal. B*, **2019**,**254**:371-379
- [17] Lei Z D, Xue Y C, Chen W Q, Lin Li, Qiu W, Zhang Y, Tang L. *Small*, **2018**,**14**:1802045
- [18] Pan Y T, Qian Y Y, Zheng X S, Chu S Q, Yang Y J, Ding C M, Wang X, Yu S H, Jiang H L. *Natl. Sci. Rev.*, **2021**,**8**:nwaa224
- [19] Cui W G, Hu T L. *Small*, **2020**,**12**:2003971
- [20] Fan H, Peng M, Strauss I. *Nat. Commun.*, **2021**,**12**:1-10
- [21] Liao B L, Li S X, Yang G P. *Inorg. Chem.*, **2021**,**60**:1839-1845
- [22] Li S X, Feng Z T, Hu Y, Wei C H, Wu H Z, Huang J. *Inorg. Chem.*, **2018**,**57**:13289-13295
- [23] Lopes T A, Queiroz L M, Torres E A, Kiperstok A. *Sci. Total Environ.*, **2020**,**720**:137593
- [24] Zaborowska E, Czerwionka K, Makinia J. *Appl. Energy*, **2021**, **282**: 116126
- [25] Kandiah M, Nilsen M H, Usseglio S, Jakobsen S, Olsbye U, Tilset M, Larabi C, Quadrelli E A, Bonino F, Lillerud K P. *Chem. Mater.*, **2010**,**22**:6632-6640
- [26] 李石雄, 黄凤兰, 莫巧玲, 廖蓓玲. *无机化学学报*, **2020**,**36**:1401-1412
LI S X, HUANG F L, MO Q L, LIAO B L. *Chinese J. Inorg. Chem.*, **2020**,**36**:1401-1412